



HAL
open science

BepiColombo Mio Observations of Low-Energy Ions During the First Mercury Flyby: Initial Results

Yuki Harada, Sae Aizawa, Yoshifumi Saito, Nicolas André, Moa Persson,
Dominique Delcourt, L. Z. Hadid, Markus Fraenz, Shoichiro Yokota, Andréi
Fedorov, et al.

► **To cite this version:**

Yuki Harada, Sae Aizawa, Yoshifumi Saito, Nicolas André, Moa Persson, et al.. BepiColombo Mio Observations of Low-Energy Ions During the First Mercury Flyby: Initial Results. *Geophysical Research Letters*, 2022, 49 (17), 10.1029/2022GL100279 . hal-03806925

HAL Id: hal-03806925

<https://cnrs.hal.science/hal-03806925>

Submitted on 8 Oct 2022

HAL is a multi-disciplinary open access archive for the deposit and dissemination of scientific research documents, whether they are published or not. The documents may come from teaching and research institutions in France or abroad, or from public or private research centers.

L'archive ouverte pluridisciplinaire **HAL**, est destinée au dépôt et à la diffusion de documents scientifiques de niveau recherche, publiés ou non, émanant des établissements d'enseignement et de recherche français ou étrangers, des laboratoires publics ou privés.

BepiColombo Mio Observations of Low-Energy Ions During the First Mercury Flyby: Initial Results

Yuki Harada¹, Sae Aizawa², Yoshifumi Saito³, Nicolas André², Moa Persson²,
Dominique Delcourt⁴, Lina Z. Hadid⁴, Markus Fraenz⁵, Shoichiro Yokota⁶,
Andréi Fedorov², Wataru Miyake⁷, Emmanuel Penou², Alain Barthe²,
Jean-André Sauvaud², Bruno Katra⁴, Shoya Matsuda⁸, Go Murakami³

¹Department of Geophysics, Graduate School of Science, Kyoto University, Kyoto, Japan

²IRAP, CNRS-UPS-CNES, Toulouse, France

³Institute of Space and Astronautical Science, Japan Aerospace Exploration Agency, Japan

⁴Laboratoire de Physique des Plasmas (LPP), CNRS, Observatoire de Paris, Sorbonne Université,

Université Paris Saclay, Ecole polytechnique, Institut Polytechnique de Paris, 91120 Palaiseau, France

⁵Max-Planck-Institute for Solar System Research, Göttingen, Germany

⁶Department of Earth and Space Science, Graduate School of Science, Osaka University, Japan

⁷Tokai University, 4-1-1 Kitakaname, Hiratsuka-shi, Kanagawa, Japan

⁸Graduate School of Natural Science and Technology, Kanazawa University, Kanazawa, Japan

Key Points:

- We present initial reports on low energy ion observations during BepiColombo's first Mercury flyby
- Mio observed large fluctuations of ion flux with time scales down to a few seconds around the magnetopause and within the magnetosphere
- Ion energy spectra obtained in the midnight magnetotail suggest the presence of an unexpectedly dense cold component

Corresponding author: Yuki Harada, haraday@kugi.kyoto-u.ac.jp

Abstract

We present initial results of low-energy ion observations from BepiColombo's first Mercury flyby. Unprecedentedly high time resolution measurements of low energy ions at Mercury by BepiColombo Mio reveal rapid (a few seconds) and large (1–2 orders of magnitude) fluctuations of ion flux around the magnetopause and within the magnetosphere. Around the magnetic equator in the pre-midnight magnetotail, Mio observed plasma sheet ions consistent with previous observations. In the midnight magnetotail near the closest approach, Mio observed the co-existence of high-energy ($\sim\text{keV}/q$) and low-energy ($<\sim 300\text{ eV}/q$) ion components. The low-energy component is inferred to be cold with a temperature well below 100 eV and have a major contribution to the total density as opposed to previously reported cold tenuous ions. Future observations by Mio will provide insights into the sources, transport, and acceleration of the newly identified ion components.

Plain Language Summary

BepiColombo, launched on 20 October 2018, is now en route to Mercury. Along its 7-year journey to the Mercury orbit insertion, BepiColombo conducted, and will conduct, nine planetary flybys in total. This paper presents brand-new observations of ions (positively charged particles) in Mercury's magnetosphere by BepiColombo Mio during its first encounter with Mercury. Thanks to high-time resolution measurements by Mio, it is revealed that ions around Mercury change dramatically and rapidly just over a few seconds. Mio also observed an unexpectedly dense ion population with low energies, for which we do not have a definitive explanation yet. Future flyby and in-orbit observations by BepiColombo will provide key information for unraveling the dynamics and sources of ions in Mercury's magnetosphere.

1 Introduction

Driven by the intense solar wind in the inner heliosphere, Mercury's magnetosphere is known to be small and dynamic. Mercury's weak dipole magnetic field of $190\text{ nT}\cdot R_M^3$ (Anderson et al., 2012), where R_M is Mercury's radius, and high solar wind dynamic pressures at Mercury's orbit ($\sim 5\text{--}10$ times higher at $0.31\text{--}0.47\text{ AU}$ than those at 1 AU) result in small spatial dimensions of the magnetosphere with an average subsolar stand-off distance of $1.45 R_M$ (Winslow et al., 2013). Consequently, time scales of magnetospheric dynamics driven by the solar wind are considerably short at Mercury (e.g., Siscoe et al., 1975). Our understanding of Mercury's magnetosphere has been greatly advanced thanks to the two previous missions to Mercury, Mariner 10 and MESSENGER, but there remain many open questions as to the plasma sources, energy and mass transport, and particle acceleration processes in Mercury's magnetosphere, and their coupling to the exosphere, surface, and interior of the planet (J. Slavin, 2004; Raines et al., 2015; W. Sun, Dewey, et al., 2022).

BepiColombo conducted its first Mercury flyby on 1 October 2021. Near the closest approach, BepiColombo traversed low-altitude regions in the southern hemisphere, which were poorly sampled, or even never visited, by Mariner 10 and MESSENGER. During the flyby, the two spacecraft of BepiColombo, Mio and Mercury Planetary Orbiter, were in a stacked configuration (Murakami et al., 2020), and the Mercury Plasma Particle Experiment (MPPE) onboard Mio successfully measured low-energy ions and electrons in the vicinity of Mercury. This paper reports on initial results from low-energy ion observations by Mio during the first Mercury flyby. A broader overview of simultaneous observations of low-energy ions and electrons in Mercury's magnetosphere by Mio will be reported elsewhere.

2 Data and Model

We analyze low-energy ion data obtained by the Mercury Ion Analyzer (MIA), one of the seven sensors of the MPPE consortium onboard Mio (Saito et al., 2021). An energy-time (Et) spectrogram with a nominal time resolution of 4 s (which is the planned spin period) is generated from the MIA “Et” data product. This data product contains ion energy spectra for four directions according to spin phase such that energy spectra will be obtained separately for ions traveling approximately sunward, anti-sunward, dawnward, and duskward in the nominal in-orbit operation (see Figure 31 and Table 12 of Saito et al. (2021)). In a given spin, a full spin period is divided into 8 groups of spin sectors, spin sector groups 0–7. MIA generates the Et product for 4 directions consisting of spin sector groups 0 and 7 (direction 1), 1 and 2 (direction 2), 3 and 4 (direction 3), and 5 and 6 (direction 4). During the cruise phase, we can exploit this functionality to effectively enhance the time resolution from 4 s down to 1 s because the spacecraft does not spin and the field of view does not change rapidly during the cruise and flyby observations. By ordering the three sequential data points, namely directions 2 through 4, according to the data acquisition times and discarding the direction 1, which accumulates non-sequential data points from the first 1/8 and last 1/8 of the spin period, we obtain “quasi-1 s” resolution data recorded at a cadence of 1 s, 1 s, 2 s, 1 s, 1 s, 2 s, and so on. Due to the ongoing calibration of the lowest energies of the MIA energy sweep, we restrict our analysis to the MIA data above 80 eV/q in this paper. We note that mass-resolved ion data from the Mass Spectrum Analyzer (MSA) are unavailable near the first closest approach to Mercury. As Mio is behind the thermal shield during the cruise phase, most of the field of view (FOV) of MIA is blocked (Murakami et al., 2020), and we need to consider its unblocked, effective FOV when interpreting the data.

To aid the interpretation of the particle data, we utilize an empirical magnetospheric magnetic field model (KT17) developed by Korth et al. (2017). The KT17 model is parameterized by the heliocentric distance of Mercury and the disturbance index (DI) of Mercury’s magnetosphere (Anderson et al., 2013). For the former, we use the instantaneous heliocentric distance at the time of the observation. For the latter, we chose DI of 100, which represents the most compressed state of the magnetosphere that can be expressed by the model, based on locations of outbound magnetopause crossings identified from the ion observations as described in the following section. We conducted tests with different choices of DI, which did not qualitatively change the results presented in this paper.

Unless otherwise noted, we use the aberrated Mercury Solar Magnetospheric (MSM) coordinate system, which takes into account the northward offset of Mercury’s dipole and the solar wind aberration according to the instantaneous orbital velocity of Mercury and a typical solar wind speed of 400 km/s in the same manner as Korth et al. (2015).

3 Observations

Figure 1 shows the observation geometry of Mio’s first Mercury flyby on 1 October 2021. As seen in Figures 1a, 1c, and 1d, the spacecraft entered the duskside magnetotail from the flank magnetosheath around 23:10 UTC, crossed the magnetic equator ($Z_{MSM} = 0$) in the pre-midnight magnetotail at 23:17:37 UTC, traveled from midnight to dawn in the southern MSM hemisphere around 23:30–23:40 UTC near the closest approach, and exited from the post-dawn magnetosphere into the dayside magnetosheath around 23:41 UTC. Magnetic field line mapping with the KT17 model suggests that the spacecraft was located on closed field lines connected to the magnetic equator at radial distances of ~ 1.7 – $4.9R_M$ (Figure 1a) and to the surface foot points near the open-closed boundary (Figure 1b).

119 Figure 2 presents the overall time series of MIA data along with predictions from
 120 the KT17 model. The white areas in Figure 2a represent data gaps. The colored labels
 121 on top of Figure 2a indicate plasma regions inferred from the ion data and the obser-
 122 vation geometry. For selected time intervals (indicated by the horizontal bars with la-
 123 bels of “3a”–“3h” in Figures 2a and 2b), we present detailed characteristics of the ion
 124 data in Figure 3. In the following, we investigate ion signatures in each region.

125 Mio was presumably located in the magnetosheath before 23:07:45 UTC. During
 126 this time interval, MIA observed a relatively low flux of ions at a few 100 eV/q (Figure
 127 2a). This signature can be interpreted as a small portion of magnetosheath ions detected
 128 by MIA’s limited FOV, which was directed mostly duskward (Figure 1a).

129 We infer that Mio crossed a transition region from the magnetosheath into the mag-
 130 netosphere during 23:07:45–23:14:06 UTC. During 23:07:45–23:09:41 UTC, MIA mea-
 131 sured intermittent flux enhancements at broad energies up to several keV/q superim-
 132 posed on the continuous presence of a few 100 eV ions (Figure 2a). Figure 3e shows a
 133 zoom-in of the intermittent flux enhancements. The durations of the individual flux en-
 134 hancements range from several seconds to a few tens of seconds, with the spacing of sim-
 135 ilar durations. Subsequently, MIA observed sustained broad energy spectra up to sev-
 136 eral keV/q along with a relatively high flux of low-energy ions at $< \sim 300$ eV/q during
 137 23:13:04–23:14:06 UTC (Figure 2a). Figure 3a shows a representative energy spectrum
 138 at this time along with a two-component (a cold Maxwellian and a hot kappa distribu-
 139 tion (Vasyliunas, 1968)) fitting result. When fitting the data, we assume that ions are
 140 isotropic and are all protons. We note that if planetary heavy ions are present, their frac-
 141 tional density is underestimated by a factor of $\sqrt{m/q}$ under the proton-only assumption
 142 (McFadden et al., 2008). In Figure 3a, it is seen that the observed spectrum is well rep-
 143 resented by a superposition of a relatively cold, dense component and a hot, tenuous com-
 144 ponent. The hot component with broad energies is likely to be magnetospheric ions. The
 145 intermittent appearance of the hot ions (Figure 3e) and the mixture of relatively cold
 146 and hot ions (Figure 3a) suggest a structured and gradual transition from the flank mag-
 147 netosheath into the low-latitude magnetotail encountered by Mio rather than a single
 148 crossing of a sharp boundary.

149 Mio crossed the magnetic equator in the pre-midnight magnetotail (Figure 1) at
 150 23:17:37 UTC (indicated by the vertical black line in Figure 2). Around this time, MIA
 151 observed broad energy spectra, presumably of plasma sheet ions (Figure 2a). Figure 3b
 152 shows an energy spectrum obtained just before the magnetic equator crossing. We ob-
 153 serve a one-component distribution well represented by a kappa distribution.

154 Next, we investigate ion signatures observed at low altitudes below 1000 km near
 155 the closest approach. Around 23:30 UTC, we observe the co-existence of two well-separated
 156 components, one at $\sim 1\text{--}3$ keV/q and the other at $< \sim 300$ eV/q (labeled “3c” in Figure
 157 2a) on field lines connected to the midnight magnetotail (Figure 1). Figure 3c shows the
 158 energy spectrum of the two-component ions. We observe two humps in the energy spec-
 159 trum, which clearly deviates from a single Maxwellian or kappa distribution. The col-
 160 ored lines show two-Maxwellian fits to the data (for this spectrum, the hot component
 161 has too few data points to be adequately fitted by a kappa distribution). The cold com-
 162 ponent is inferred to have a low temperature (well below 100 eV) and relatively high den-
 163 sity compared to the hot component. After the hot component disappeared at 23:30:20
 164 UTC, a similar two-component signature reemerged around 23:32 UTC, and subsequently,
 165 the hot and cold components merged into one component at broad energies of $\sim 100\text{--}3000$
 166 eV/q (labeled “3d” in Figure 2a). As shown in Figure 3d, the merged component is char-
 167 acterized by a single Maxwellian-like distribution with a large kappa value.

168 The MIA quasi-1 s data reveal that the \sim keV/q ion component comprises finer sub-
 169 structures. Figures 3f and 3g show zoom-ins of flux variations at representative energies
 170 (during the time intervals labeled “3f” and “3g” in Figure 2b). In the quasi-1 s data, we

171 observe large, rapid flux fluctuations with ~ 1 – 2 orders of magnitude variations within
 172 just a few seconds. This time scale of the rapid flux variations corresponds to several pro-
 173 ton gyroperiods and to a fraction of the gyroradius divided by the spacecraft velocity
 174 (see the horizontal bars in Figures 3f and 3g). Thus, if these substructures originate en-
 175 tirely from temporal variations, they represent proton-scale time variations. If the ob-
 176 served variations are purely spatial and result from crossings of static structures, they
 177 represent sub-proton-scale spatial structures (see Figure 2e for ion gyroradii in kilome-
 178 ters).

179 We also observe signatures suggestive of absorption of magnetospheric ions by the
 180 surface of Mercury. Between the two vertical dashed lines in Figures 2a and 2b, the ob-
 181 served ion flux is reduced by a factor of >10 compared to that at the adjacent times. The
 182 reduced ion flux coincides with the time interval during which the effective FOV of MIA
 183 is predicted to be within the loss cone according to the KT17 model (Figure 2c). The
 184 predicted size of the loss cone is relatively large because of the strong local magnetic fields
 185 at low altitudes (Figures 2d and 2e).

186 We next examine the outbound magnetopause crossing. Overall, the peak energy
 187 shifted from ~ 1 keV/q down to ~ 200 eV/q during 23:40:30–23:41:10 UTC (Figure 2a).
 188 The ~ 1 keV/q peak energy is consistent with the ion population observed well within
 189 the magnetosphere. The relatively low energy peak at ~ 200 eV/q and intense ion flux
 190 exceeding 10^8 eV/cm²/s/sr/eV observed after 23:41:00 UTC suggest that the spacecraft
 191 crossed the magnetopause into the magnetosheath. Note that the direction of MIA’s FOV
 192 is more favorable for detection of the bulk component of magnetosheath ion flows de-
 193 flected along the magnetopause in the outbound magnetosheath as opposed to the in-
 194 bound magnetosheath (Figure 1). Figure 3h presents the time variation of 210 eV/q ion
 195 flux around the inferred magnetopause crossing. The MIA data clearly resolve multiple
 196 crossings, exhibiting at least 3 crossings within a 40 s interval.

197 4 Discussion

198 We now discuss Mio’s observations of low-energy ions in comparison with relevant
 199 observations at Mercury by the two previous missions, Mariner 10 and MESSENGER,
 200 and provide implications for future observations by BepiColombo.

201 Around the magnetic equator in the pre-midnight magnetotail, MIA observed a broad
 202 energy spectrum characterized by a kappa distribution with a density of ~ 16 cm⁻³, tem-
 203 perature of ~ 470 eV, and kappa of ~ 4.8 (Figure 3b). These parameters are generally
 204 in accordance with previously reported results (Gershman et al., 2014; Zhao et al., 2020).
 205 Specifically, the density (temperature) is near the higher (lower) end of the MESSEN-
 206 GER observations in the pre-midnight plasma sheet reported by Gershman et al. (2014).
 207 They also reported that the high-density, low-temperature plasma sheet tends to be ob-
 208 served under slower (and generally denser) solar wind conditions. According to Figure
 209 1 of Gershman et al. (2014), the MIA observation of relatively cold (~ 470 eV ~ 5.5 MK),
 210 dense (~ 16 cm⁻³) plasma sheet may indirectly imply a slow ($< \sim 300$ km/s) and gener-
 211 ally dense condition of the upstream solar wind during the flyby.

212 MIA measured the two components of high-energy (~ 1 keV/q) and low-energy ($< \sim 300$
 213 eV/q) ions (Figure 3c) around midnight in the magnetotail. The cold component pro-
 214 vides a predominant contribution to the total density (Figure 3c) as opposed to the re-
 215 portedly small cold to total density ratios ($\sim 10\%$) based on case studies (W. J. Sun et
 216 al., 2017) and average proton energy spectra in various spatial regions sampled by MES-
 217 SENGGER (Zhao et al., 2020). The two-component energy spectra observed by MIA are
 218 reminiscent of multiple ion beams observed in the terrestrial Plasma Sheet Boundary Layer
 219 (PSBL) (Eastman et al., 1984, 1985; Nakamura et al., 1992; Hirahara et al., 1994; Parks
 220 et al., 2001). In the terrestrial PSBL, the high-energy component often represents a high-

221 speed ion flow, while the low-energy component comprises cold ions of ionospheric ori-
 222 gin. In this regard, a notable difference between Mercury and Earth is the lack of a sig-
 223 nificant ionospheric source at Mercury. The sources of magnetospheric plasma at Mer-
 224 cury are thought to be mainly provided by the entry of the solar wind plasma (Sundberg
 225 et al., 2012; Korth et al., 2014; DiBraccio, Slavin, Raines, et al., 2015; Jasinski et al., 2017)
 226 with a minor number density contribution from planetary heavy ions on average (Gershman
 227 et al., 2014). Thus, the cold dense component could be either a low-energy portion of
 228 magnetosheath ions that are transported to the low-altitude midnight magnetotail or plan-
 229 etary heavy ions that are denser than previously thought. To elucidate the sources and
 230 transport processes of the two-component ions, 3D velocity distribution functions and
 231 ion composition should be investigated in detail, much as done for the terrestrial mag-
 232 netotail. It is also remarkable that the hot component ions exhibit large variability over
 233 several proton gyroperiods in time and within a fraction of the proton gyroradius in space,
 234 implying their fundamentally kinetic nature. There appear to be plenty of possible drivers
 235 of the rapid ion flux variations in Mercury’s magnetosphere, which contains a variety of
 236 rapid ($< \sim 10$ s) fluctuations such as flux transfer events (FTEs) (e.g., J. A. Slavin et al.,
 237 2012), magnetotail flux ropes (e.g., DiBraccio, Slavin, Imber, et al., 2015), cross-tail cur-
 238 rent sheet flapping (Poh et al., 2020; Zhang et al., 2020), and Pi2-like pulsations (W.-
 239 J. Sun et al., 2015). The properties of the relatively dense, cold ions and the highly vari-
 240 able, hot ions in Mercury’s magnetosphere should be systematically investigated with
 241 future observations.

242 Neither of the inbound and outbound magnetopause crossings was a simple, sin-
 243 gle crossing of a sharp boundary. The high-time-resolution ion measurements by MIA
 244 indicate complex and rapid variations of ions of magnetosheath and magnetospheric ori-
 245 gins. Rapid, multiple magnetopause crossings at Mercury have been identified and an-
 246 alyzed mainly by high-time resolution magnetic field measurements, and were interpreted
 247 as quick relative motion of the magnetopause (Ness et al., 1974; DiBraccio et al., 2013;
 248 J. A. Slavin et al., 2014) and as a spatially structured and temporally evolving bound-
 249 ary such as Kelvin-Helmholtz waves and FTEs at the magnetopause (J. A. Slavin et al.,
 250 2008, 2012; Sundberg et al., 2012; Liljeblad et al., 2014; Gershman et al., 2015; Aizawa
 251 et al., 2020). Combination of high-time-resolution ion and magnetic field measurements
 252 by BepiColombo will shed new light on the dynamics of the magnetospheric boundaries
 253 at Mercury.

254 During the time interval in which the MIA FOV is directed within the loss cone
 255 predicted by the KT17 model, the ion flux measured by MIA is >10 times lower than
 256 that at the adjacent times. This is in agreement with the ion loss cone observed by MES-
 257 SENDER within Mercury’s magnetosphere (Winslow et al., 2014; Zhao et al., 2020, 2022),
 258 though we cannot conclusively confirm the ion loss cone from the flyby MIA data due
 259 to the limited FOV. In-orbit observations by MIA will provide the full 4π coverage, and
 260 in combination with magnetic field measurements, comprehensive energy–pitch-angle dis-
 261 tributions of ions will be available. Such data will enable ion reflectometry to remotely
 262 probe the surface magnetic field strength (Winslow et al., 2014) and possibly electrostatic
 263 potentials (Harada et al., 2017), as well as investigate surface-emitted ions such as backscat-
 264 tered and sputtered ions (Saito et al., 2008; Yokota et al., 2009; Raines et al., 2014; W. Sun,
 265 Slavin, et al., 2022).

266 5 Conclusions

267 This paper presents initial reports on low-energy ion measurements by Mio dur-
 268 ing the first Mercury flyby. The high-time resolution data obtained by MIA highlight
 269 the dynamic nature of low-energy ions in Mercury’s magnetosphere. Both of the inbound
 270 and outbound magnetopause crossings show the complex behavior of magnetosheath and
 271 magnetospheric ions as opposed to a simple, sharp boundary singly crossed by the space-
 272 craft. Around the magnetic equator in the pre-midnight magnetotail, MIA observed plasma

273 sheet ions with broad energies. The inferred density (temperature) of the pre-midnight
 274 plasma sheet ions is near the higher (lower) end of the reported range of the MESSEN-
 275 GER results, possibly resulting from a generally slow and dense condition of the upstream
 276 solar wind. In the midnight magnetosphere, MIA observed the co-existence of high-energy
 277 (\sim keV/q) and low-energy ($< \sim 300$ eV/q) components. The low-energy component is
 278 inferred to be cold ($T < 100$ eV) and have a major contribution to the total density
 279 in contrast to the previous results suggesting only a minor density contribution by cold
 280 ions. The hot ion flux shows ~ 1 – 2 orders of magnitude variations just over a few sec-
 281 onds, suggesting the presence of proton-scale time variations and/or sub-proton-scale spa-
 282 tial structures. The sources, transport mechanisms, and acceleration processes of the two-
 283 component ions remain elusive. As demonstrated by the rich information derived from
 284 Mio’s particle measurements with the still limited capabilities during the first flyby, fu-
 285 ture flyby and in-orbit observations by BepiColombo will provide revolutionary data for
 286 understanding the structure and dynamics of Mercury’s magnetosphere.

287 6 Open Research

288 The MIA data used in this paper are archived and publicly available (Harada et
 289 al., 2022).

290 Acknowledgments

291 French co-authors acknowledge the support of CNES for the BepiColombo mission. MP
 292 is funded by the European Union’s Horizon 2020 programme under grant agreement No
 293 871149 for Europlanet 2024 RI.

294 References

- 295 Aizawa, S., Raines, J. M., Delcourt, D., Terada, N., & André, N. (2020). Messenger
 296 observations of planetary ion characteristics in the vicinity of kelvin-helmholtz
 297 vortices at mercury. *Journal of Geophysical Research: Space Physics*, *125*(10),
 298 e2020JA027871. Retrieved from [https://agupubs.onlinelibrary.wiley](https://agupubs.onlinelibrary.wiley.com/doi/abs/10.1029/2020JA027871)
 299 [.com/doi/abs/10.1029/2020JA027871](https://doi.org/10.1029/2020JA027871) (e2020JA027871 2020JA027871) doi:
 300 <https://doi.org/10.1029/2020JA027871>
- 301 Anderson, B. J., Johnson, C. L., & Korth, H. (2013). A magnetic disturbance
 302 index for Mercury’s magnetic field derived from MESSENGER Magnetome-
 303 ter data. *Geochem. Geophys. Geosyst.*, *14*(9), 3875–3886. Retrieved from
 304 <http://dx.doi.org/10.1002/ggge.20242> doi: 10.1002/ggge.20242
- 305 Anderson, B. J., Johnson, C. L., Korth, H., Winslow, R. M., Borovsky, J. E., Pu-
 306 rucker, M. E., . . . McNutt, R. L. (2012). Low-degree structure in Mer-
 307 cury’s planetary magnetic field. *J. Geophys. Res.*, *117*, E00L12. doi:
 308 10.1029/2012JE004159
- 309 DiBraccio, G. A., Slavin, J. A., Boardsen, S. A., Anderson, B. J., Korth, H., Zur-
 310 buchen, T. H., . . . Solomon, S. C. (2013). MESSENGER observations of
 311 magnetopause structure and dynamics at Mercury. *J. Geophys. Res.*, *118*(3),
 312 997–1008. Retrieved from <http://dx.doi.org/10.1002/jgra.50123> doi:
 313 10.1002/jgra.50123
- 314 DiBraccio, G. A., Slavin, J. A., Imber, S. M., Gershman, D. J., Raines, J. M., Jack-
 315 man, C. M., . . . Solomon, S. C. (2015).
 316 *Planet. Space Sci.*, *115*, 77 - 89. Retrieved from [http://www.sciencedirect](http://www.sciencedirect.com/science/article/pii/S0032063314004085)
 317 [.com/science/article/pii/S0032063314004085](http://www.sciencedirect.com/science/article/pii/S0032063314004085) doi: 10.1016/j.pss.2014.12
 318 .016
- 319 DiBraccio, G. A., Slavin, J. A., Raines, J. M., Gershman, D. J., Tracy, P. J.,
 320 Boardsen, S. A., . . . Solomon, S. C. (2015). First observations of Mer-
 321 cury’s plasma mantle by MESSENGER. *Geophys. Res. Lett.*, *42*(22), 9666–

- 322 9675. Retrieved from <http://dx.doi.org/10.1002/2015GL065805> doi:
323 10.1002/2015GL065805
- 324 Eastman, T. E., Frank, L. A., & Huang, C. Y. (1985). The boundary layers as the
325 primary transport regions of the earth's magnetotail. *Journal of Geophys-
326 ical Research: Space Physics*, 90(A10), 9541-9560. Retrieved from [https://
327 agupubs.onlinelibrary.wiley.com/doi/abs/10.1029/JA090iA10p09541](https://agupubs.onlinelibrary.wiley.com/doi/abs/10.1029/JA090iA10p09541)
328 doi: <https://doi.org/10.1029/JA090iA10p09541>
- 329 Eastman, T. E., Frank, L. A., Peterson, W. K., & Lennartsson, W. (1984). The
330 plasma sheet boundary layer. *Journal of Geophysical Research: Space Physics*,
331 89(A3), 1553-1572. Retrieved from [https://agupubs.onlinelibrary.wiley
332 .com/doi/abs/10.1029/JA089iA03p01553](https://agupubs.onlinelibrary.wiley.com/doi/abs/10.1029/JA089iA03p01553) doi: [https://doi.org/10.1029/
JA089iA03p01553](https://doi.org/10.1029/
333 JA089iA03p01553)
- 334 Gershman, D. J., Raines, J. M., Slavin, J. A., Zurbuchen, T. H., Sundberg, T.,
335 Boardsen, S. A., ... Solomon, S. C. (2015). Messenger observations of
336 multiscale kelvin-helmholtz vortices at mercury. *Journal of Geophysical
337 Research: Space Physics*, 120(6), 4354-4368. Retrieved from [https://
338 agupubs.onlinelibrary.wiley.com/doi/abs/10.1002/2014JA020903](https://agupubs.onlinelibrary.wiley.com/doi/abs/10.1002/2014JA020903) doi:
339 <https://doi.org/10.1002/2014JA020903>
- 340 Gershman, D. J., Slavin, J. A., Raines, J. M., Zurbuchen, T. H., Anderson, B. J.,
341 Korth, H., ... Solomon, S. C. (2014). Ion kinetic properties in mercury's
342 pre-midnight plasma sheet. *Geophysical Research Letters*, 41(16), 5740-5747.
343 Retrieved from [https://agupubs.onlinelibrary.wiley.com/doi/abs/
344 10.1002/2014GL060468](https://agupubs.onlinelibrary.wiley.com/doi/abs/10.1002/2014GL060468) doi: <https://doi.org/10.1002/2014GL060468>
- 345 Harada, Y., Aizawa, S., Saito, Y., André, N., Persson, M., Delcourt, D., ... Mu-
346 rakami, G. (2022, July). *BepiColombo Mio MIA Data During the First
347 Mercury Flyby*. Zenodo. Retrieved from [https://doi.org/10.5281/
348 zenodo.6797894](https://doi.org/10.5281/zenodo.6797894) doi: 10.5281/zenodo.6797894
- 349 Harada, Y., Poppe, A. R., Halekas, J. S., Chamberlin, P. C., & McFadden, J. P.
350 (2017). Photoemission and electrostatic potentials on the dayside lunar sur-
351 face in the terrestrial magnetotail lobes. *Geophys. Res. Lett.*, 44(11), 5276-
352 5282. Retrieved from <http://dx.doi.org/10.1002/2017GL073419> doi:
353 10.1002/2017GL073419
- 354 Hirahara, M., Nakamura, M., Terasawa, T., Mukai, T., Saito, Y., Yamamoto,
355 T., ... Kokubun, S. (1994). Acceleration and heating of cold ion
356 beams in the plasma sheet boundary layer observed with geotail. *Geo-
357 physical Research Letters*, 21(25), 3003-3006. Retrieved from [https://
358 agupubs.onlinelibrary.wiley.com/doi/abs/10.1029/94GL02109](https://agupubs.onlinelibrary.wiley.com/doi/abs/10.1029/94GL02109) doi:
359 <https://doi.org/10.1029/94GL02109>
- 360 Jasinski, J. M., Slavin, J. A., Raines, J. M., & DiBraccio, G. A. (2017). Mer-
361 cury's solar wind interaction as characterized by magnetospheric plasma
362 mantle observations with messenger. *Journal of Geophysical Research:
363 Space Physics*, 122(12), 12,153-12,169. Retrieved from [https://agupubs
364 .onlinelibrary.wiley.com/doi/abs/10.1002/2017JA024594](https://agupubs.onlinelibrary.wiley.com/doi/abs/10.1002/2017JA024594) doi:
365 <https://doi.org/10.1002/2017JA024594>
- 366 Korth, H., Anderson, B. J., Gershman, D. J., Raines, J. M., Slavin, J. A., Zur-
367 buchen, T. H., ... McNutt Jr., R. L. (2014). Plasma distribution in
368 mercury's magnetosphere derived from messenger magnetometer and fast
369 imaging plasma spectrometer observations. *Journal of Geophysical Re-
370 search: Space Physics*, 119(4), 2917-2932. Retrieved from [https://
371 agupubs.onlinelibrary.wiley.com/doi/abs/10.1002/2013JA019567](https://agupubs.onlinelibrary.wiley.com/doi/abs/10.1002/2013JA019567) doi:
372 <https://doi.org/10.1002/2013JA019567>
- 373 Korth, H., Johnson, C. L., Philpott, L., Tsyganenko, N. A., & Anderson, B. J.
374 (2017). A Dynamic Model of Mercury's Magnetospheric Magnetic Field.
375 *Geophys. Res. Lett.*, 44(20), 10,147-10,154. Retrieved from [https://
376 agupubs.onlinelibrary.wiley.com/doi/abs/10.1002/2017GL074699](https://agupubs.onlinelibrary.wiley.com/doi/abs/10.1002/2017GL074699) doi:

- 377 10.1002/2017GL074699
- 378 Korth, H., Tsyganenko, N. A., Johnson, C. L., Philpott, L. C., Anderson, B. J.,
379 Al Asad, M. M., ... McNutt, R. L. (2015). Modular model for Mercury's
380 magnetospheric magnetic field confined within the average observed magne-
381 topause. *J. Geophys. Res.*, *120*(6), 4503-4518. Retrieved from [https://](https://agupubs.onlinelibrary.wiley.com/doi/abs/10.1002/2015JA021022)
382 agupubs.onlinelibrary.wiley.com/doi/abs/10.1002/2015JA021022 doi:
383 10.1002/2015JA021022
- 384 Liljeblad, E., Sundberg, T., Karlsson, T., & Kullen, A. (2014). Statistical investiga-
385 tion of Kelvin-Helmholtz waves at the magnetopause of Mercury. *J. Geophys.*
386 *Res.*, *119*(12), 9670-9683. Retrieved from [https://agupubs.onlinelibrary](https://agupubs.onlinelibrary.wiley.com/doi/abs/10.1002/2014JA020614)
387 [.wiley.com/doi/abs/10.1002/2014JA020614](https://agupubs.onlinelibrary.wiley.com/doi/abs/10.1002/2014JA020614) doi: 10.1002/2014JA020614
- 388 McFadden, J. P., Carlson, C. W., Larson, D., Bonnell, J., Mozer, F., Angelopou-
389 los, V., ... Auster, U. (2008, DEC). THEMIS ESA First Science Results
390 and Performance Issues [Review]. *Space Sci. Rev.*, *141*(1-4), 477-508. doi:
391 {10.1007/s11214-008-9433-1}
- 392 Murakami, G., Hayakawa, H., Ogawa, H., Matsuda, S., Seki, T., Kasaba, Y., ...
393 Fujimoto, M. (2020). Mio—first comprehensive exploration of mercury's
394 space environment: Mission overview. *Space Science Reviews*, *216*(7), 113.
395 Retrieved from <https://doi.org/10.1007/s11214-020-00733-3> doi:
396 10.1007/s11214-020-00733-3
- 397 Nakamura, M., Paschmann, G., Baumjohann, W., & Sckopke, N. (1992). Ion dis-
398 tributions and flows in and near the plasma sheet boundary layer. *Journal*
399 *of Geophysical Research: Space Physics*, *97*(A2), 1449-1460. Retrieved from
400 <https://agupubs.onlinelibrary.wiley.com/doi/abs/10.1029/91JA02361>
401 doi: <https://doi.org/10.1029/91JA02361>
- 402 Ness, N. F., Behannon, K. W., Lepping, R. P., Whang, Y. C., & Schatten, K. H.
403 (1974). Magnetic Field Observations near Mercury: Preliminary Re-
404 sults from Mariner 10. *Science*, *185*(4146), 151-160. Retrieved from
405 <http://www.sciencemag.org/content/185/4146/151.abstract> doi:
406 10.1126/science.185.4146.151
- 407 Parks, G. K., Chen, L. J., Fillingim, M., & McCarthy, M. (2001). Kinetic character-
408 ization of plasma sheet dynamics. *Space Science Reviews*, *95*(1), 237-255. Re-
409 trieved from <https://doi.org/10.1023/A:1005206701965> doi: 10.1023/A:
410 1005206701965
- 411 Poh, G., Sun, W., Clink, K. M., Slavin, J. A., Dewey, R. M., Jia, X., ... Espley,
412 J. R. (2020). Large-amplitude oscillatory motion of mercury's cross-tail
413 current sheet. *Journal of Geophysical Research: Space Physics*, *125*(7),
414 e2020JA027783. Retrieved from [https://agupubs.onlinelibrary.wiley](https://agupubs.onlinelibrary.wiley.com/doi/abs/10.1029/2020JA027783)
415 [.com/doi/abs/10.1029/2020JA027783](https://agupubs.onlinelibrary.wiley.com/doi/abs/10.1029/2020JA027783) (e2020JA027783 2020JA027783) doi:
416 <https://doi.org/10.1029/2020JA027783>
- 417 Raines, J. M., DiBraccio, G. A., Cassidy, T. A., Delcourt, D. C., Fujimoto, M.,
418 Jia, X., ... Wurz, P. (2015). Plasma sources in planetary magnetospheres:
419 Mercury. *Space Science Reviews*, *192*(1), 91-144. Retrieved from [https://](https://doi.org/10.1007/s11214-015-0193-4)
420 doi.org/10.1007/s11214-015-0193-4 doi: 10.1007/s11214-015-0193-4
- 421 Raines, J. M., Gershman, D. J., Slavin, J. A., Zurbuchen, T. H., Korth, H., Ander-
422 son, B. J., & Solomon, S. C. (2014). Structure and dynamics of Mercury's
423 magnetospheric cusp: MESSENGER measurements of protons and plane-
424 tary ions. *J. Geophys. Res.*, *119*(8), 6587-6602. Retrieved from [https://](https://agupubs.onlinelibrary.wiley.com/doi/abs/10.1002/2014JA020120)
425 agupubs.onlinelibrary.wiley.com/doi/abs/10.1002/2014JA020120 doi:
426 10.1002/2014JA020120
- 427 Saito, Y., Delcourt, D., Hirahara, M., Barabash, S., André, N., Takashima, T.,
428 ... Team, B. M. (2021). Pre-flight calibration and near-earth commission-
429 ing results of the mercury plasma particle experiment (mppe) onboard mmo
430 (mio). *Space Science Reviews*, *217*(5), 70. Retrieved from [https://doi.org/](https://doi.org/10.1007/s11214-021-00839-2)
431 [10.1007/s11214-021-00839-2](https://doi.org/10.1007/s11214-021-00839-2) doi: 10.1007/s11214-021-00839-2

- 432 Saito, Y., Yokota, S., Tanaka, T., Asamura, K., Nishino, M. N., Fujimoto, M., ...
 433 Terasawa, T. (2008). Solar Wind Proton Reflection at the Lunar Surface:
 434 Low Energy Ion Measurement by MAP-PACE Onboard SELENE (KAGUYA).
 435 *Geophys. Res. Lett.*, *35*, L24205. doi: 10.1029/2008GL036077
- 436 Siscoe, G. L., Ness, N. F., & Yeates, C. M. (1975). Substorms on Mercury?
 437 *J. Geophys. Res.*, *80*(31), 4359-4363. Retrieved from [https://agupubs](https://agupubs.onlinelibrary.wiley.com/doi/abs/10.1029/JA080i031p04359)
 438 [.onlinelibrary.wiley.com/doi/abs/10.1029/JA080i031p04359](https://agupubs.onlinelibrary.wiley.com/doi/abs/10.1029/JA080i031p04359) doi:
 439 10.1029/JA080i031p04359
- 440 Slavin, J. (2004). Mercury's magnetosphere. *Adv. Space Res.*, *33*(11), 1859
 441 - 1874. Retrieved from [http://www.sciencedirect.com/science/article/](http://www.sciencedirect.com/science/article/pii/S0273117704000092)
 442 [pii/S0273117704000092](http://www.sciencedirect.com/science/article/pii/S0273117704000092) doi: 10.1016/j.asr.2003.02.019
- 443 Slavin, J. A., Acuña, M. H., Anderson, B. J., Baker, D. N., Benna, M., Gloeck-
 444 ler, G., ... Zurbuchen, T. H. (2008). Mercury's Magnetosphere After
 445 MESSENGER's First Flyby. *Science*, *321*(5885), 85-89. Retrieved from
 446 <http://www.sciencemag.org/content/321/5885/85.abstract> doi:
 447 10.1126/science.1159040
- 448 Slavin, J. A., DiBraccio, G. A., Gershman, D. J., Imber, S. M., Poh, G. K., Raines,
 449 J. M., ... Solomon, S. C. (2014). MESSENGER observations of Mercury's
 450 dayside magnetosphere under extreme solar wind conditions. *J. Geophys. Res.*,
 451 *119*(10), 8087-8116. Retrieved from [https://agupubs.onlinelibrary.wiley](https://agupubs.onlinelibrary.wiley.com/doi/abs/10.1002/2014JA020319)
 452 [.com/doi/abs/10.1002/2014JA020319](https://agupubs.onlinelibrary.wiley.com/doi/abs/10.1002/2014JA020319) doi: 10.1002/2014JA020319
- 453 Slavin, J. A., Imber, S. M., Boardsen, S. A., DiBraccio, G. A., Sundberg, T., Saran-
 454 tos, M., ... Solomon, S. C. (2012, OCT 30). MESSENGER observations
 455 of a flux-transfer-event shower at Mercury [Article]. *J. Geophys. Res.*, *117*,
 456 A00M06. doi: {10.1029/2012JA017926}
- 457 Sun, W., Dewey, R. M., Aizawa, S., Huang, J., Slavin, J. A., Fu, S., ... Bowers,
 458 C. F. (2022). Review of mercury's dynamic magnetosphere: Post-messenger
 459 era and comparative magnetospheres. *Science China Earth Sciences*, *65*(1),
 460 25-74. Retrieved from <https://doi.org/10.1007/s11430-021-9828-0> doi:
 461 10.1007/s11430-021-9828-0
- 462 Sun, W., Slavin, J. A., Milillo, A., Dewey, R. M., Orsini, S., Jia, X., ... Li, C.
 463 (2022). Messenger observations of planetary ion enhancements at mercury's
 464 northern magnetospheric cusp during flux transfer event showers. *Journal*
 465 *of Geophysical Research: Space Physics*, *127*(4), e2022JA030280. Retrieved
 466 from [https://agupubs.onlinelibrary.wiley.com/doi/abs/10.1029/](https://agupubs.onlinelibrary.wiley.com/doi/abs/10.1029/2022JA030280)
 467 [2022JA030280](https://agupubs.onlinelibrary.wiley.com/doi/abs/10.1029/2022JA030280) (e2022JA030280 2022JA030280) doi: [https://doi.org/10.1029/](https://doi.org/10.1029/2022JA030280)
 468 [2022JA030280](https://doi.org/10.1029/2022JA030280)
- 469 Sun, W. J., Raines, J. M., Fu, S. Y., Slavin, J. A., Wei, Y., Poh, G. K., ... Wan,
 470 W. X. (2017). Messenger observations of the energization and heating of pro-
 471 tons in the near-mercury magnetotail. *Geophysical Research Letters*, *44*(16),
 472 8149-8158. Retrieved from [https://agupubs.onlinelibrary.wiley.com/](https://agupubs.onlinelibrary.wiley.com/doi/abs/10.1002/2017GL074276)
 473 [doi/abs/10.1002/2017GL074276](https://agupubs.onlinelibrary.wiley.com/doi/abs/10.1002/2017GL074276) doi: 10.1002/2017GL074276
- 474 Sun, W.-J., Slavin, J. A., Fu, S., Raines, J. M., Sundberg, T., Zong, Q.-G., ... Zur-
 475 buchen, T. H. (2015). Messenger observations of alfvénic and compressional
 476 waves during mercury's substorms. *Geophysical Research Letters*, *42*(15), 6189-
 477 6198. Retrieved from [https://agupubs.onlinelibrary.wiley.com/doi/abs/](https://agupubs.onlinelibrary.wiley.com/doi/abs/10.1002/2015GL065452)
 478 [10.1002/2015GL065452](https://agupubs.onlinelibrary.wiley.com/doi/abs/10.1002/2015GL065452) doi: <https://doi.org/10.1002/2015GL065452>
- 479 Sundberg, T., Boardsen, S. A., Slavin, J. A., Anderson, B. J., Korth, H., Zur-
 480 buchen, T. H., ... Solomon, S. C. (2012). MESSENGER orbital obser-
 481 vations of large-amplitude Kelvin-Helmholtz waves at Mercury's magne-
 482 topause. *J. Geophys. Res.*, *117*(A4), A04216. Retrieved from [https://](https://agupubs.onlinelibrary.wiley.com/doi/abs/10.1029/2011JA017268)
 483 agupubs.onlinelibrary.wiley.com/doi/abs/10.1029/2011JA017268 doi:
 484 10.1029/2011JA017268
- 485 Vasyliunas, V. (1968). A Survey of Low-Energy Electrons in the Evening Sector of
 486 the Magnetosphere with OGO 1 and OGO 3 [Article]. *J. Geophys. Res.*, *73*(9),

Figure 1. BepiColombo trajectory (a) projected on the $X_{\text{MSM}}-Y_{\text{MSM}}$ plane, (b) mapped to the planet surface along magnetic field lines predicted from the KT17 model (Korth et al., 2017) as a function of the foot point MLT and the foot point geographic latitude, and projected on the (c) $X_{\text{MSM}}-Z_{\text{MSM}}$ and (d) $Y_{\text{MSM}}-Z_{\text{MSM}}$ planes. The curved line labeled “B-line magnetic equator mapping” in Figure 1a shows a magnetic field line mapping to the magnetic equator ($Z_{\text{MSM}} = 0$). We use the instantaneous heliocentric distance and a disturbance index (DI) of 100 as input parameters for the KT17 model. In Figures 1a, 1c, and 1d, the colored, thin curves show the KT17 model field lines traced from the spacecraft position, and the black fans indicate the effective field of view of MIA during the observation. The gray curve in Figure 1a shows the KT17 model magnetopause. The dashed line in Figure 1b shows the open-closed boundary at which the traced field line distance exceeds $10R_M$ (Korth et al., 2014). The gray curves in Figure 1c show the KT17 model field lines on the $X_{\text{MSM}}-Z_{\text{MSM}}$ plane.

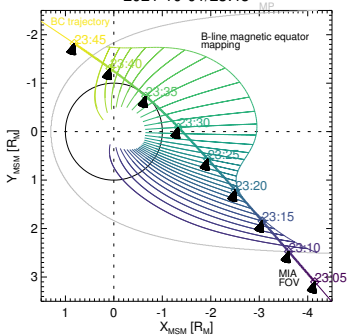
- 487 2839-2884. doi: {10.1029/JA073i009p02839}
- 488 Winslow, R. M., Anderson, B. J., Johnson, C. L., Slavin, J. A., Korth, H., Purucker,
489 M. E., ... Solomon, S. C. (2013). Mercury’s magnetopause and bow shock
490 from MESSENGER Magnetometer observations. *J. Geophys. Res.*, *118*(5),
491 2213-2227. Retrieved from [https://agupubs.onlinelibrary.wiley.com/
492 doi/abs/10.1002/jgra.50237](https://agupubs.onlinelibrary.wiley.com/doi/abs/10.1002/jgra.50237) doi: 10.1002/jgra.50237
- 493 Winslow, R. M., Johnson, C. L., Anderson, B. J., Gershman, D. J., Raines, J. M.,
494 Lillis, R. J., ... Zuber, M. T. (2014). Mercury’s surface magnetic field de-
495 termined from proton-reflection magnetometry. *Geophys. Res. Lett.*, *41*(13),
496 4463-4470. Retrieved from <http://dx.doi.org/10.1002/2014GL060258> doi:
497 10.1002/2014GL060258
- 498 Yokota, S., Saito, Y., Asamura, K., Tanaka, T., Nishino, M. N., Tsunakawa, H., ...
499 Terasawa, T. (2009). First Direct Detection of Ions Originating from the Moon
500 by MAP-PACE IMA Onboard SELENE (KAGUYA). *Geophys. Res. Lett.*, *36*,
501 L11201. doi: 10.1029/2009GL038185
- 502 Zhang, C., Rong, Z. J., Gao, J. W., Zhong, J., Chai, L. H., Wei, Y., ... Wan, W. X.
503 (2020). The flapping motion of mercury’s magnetotail current sheet: Mes-
504 senger observations. *Geophysical Research Letters*, *47*(4), e2019GL086011.
505 Retrieved from [https://agupubs.onlinelibrary.wiley.com/doi/abs/
506 10.1029/2019GL086011](https://agupubs.onlinelibrary.wiley.com/doi/abs/10.1029/2019GL086011) (e2019GL086011 2019GL086011) doi: [https://
507 doi.org/10.1029/2019GL086011](https://doi.org/10.1029/2019GL086011)
- 508 Zhao, J.-T., Zong, Q.-G., Slavin, J. A., Sun, W.-J., Zhou, X.-Z., Yue, C., ... Ip,
509 W.-H. (2020). Proton properties in mercury’s magnetotail: A statisti-
510 cal study. *Geophysical Research Letters*, *47*(19), e2020GL088075. Re-
511 trieved from [https://agupubs.onlinelibrary.wiley.com/doi/abs/
512 10.1029/2020GL088075](https://agupubs.onlinelibrary.wiley.com/doi/abs/10.1029/2020GL088075) (e2020GL088075 10.1029/2020GL088075) doi:
513 <https://doi.org/10.1029/2020GL088075>
- 514 Zhao, J. T., Zong, Q. G., Yue, C., Sun, W. J., Zhang, H., Zhou, X. Z., ... Wei, Y.
515 (2022). Observational evidence of ring current in the magnetosphere of mer-
516 cury. *Nature Communications*, *13*(1), 924. Retrieved from [https://doi.org/
517 10.1038/s41467-022-28521-3](https://doi.org/10.1038/s41467-022-28521-3) doi: 10.1038/s41467-022-28521-3

Figure 2. BepiColombo Mio observations of low-energy ions during the first Mercury flyby. (a) Energy-time spectrogram of ions in units of differential energy flux ($\text{eV}/\text{cm}^2/\text{s}/\text{sr}/\text{eV}$) obtained by MIA with its nominal 4 s resolution, (b) quasi-1 s resolution data that are available only during the cruise phase, KT17 model predictions (Korth et al., 2017) of (c) pitch angle coverage of the effective field of view of MIA (black) and critical pitch angles of parallel and anti-parallel loss cones (magenta), (d) three components and magnitude of the magnetospheric magnetic field, and (e) gyroradii of 1 keV H^+ (blue) and Na^+ (red) ions as well as the spacecraft altitudes (black). The text label indicates the magnetic local time (MLT) and magnetic latitude (MLat) of the spacecraft position in the aberrated Mercury Solar Magnetospheric (MSM) coordinates as defined in Anderson et al. (2013). The horizontal bars in Figures 2a and 2b indicate the time intervals analyzed in detail in Figure 3.

Figure 3. Detailed analyses of MIA data. Ion energy spectra obtained during (a) 23:13:26–23:13:42 UTC, (b) 23:16:20–23:16:36 UTC, (c) 23:30:00–23:30:16 UTC, and (d) 23:32:33–23:32:49 UTC. The colored lines show Maxwellian and kappa distribution fits to the data under the assumption of isotropy, proton-only composition, and a constant background (which is estimated from the average count rate at the two highest energy channels during 23:29–23:25 UTC). Two component distributions are assumed for Figures 3a (a cold Maxwellian and a hot kappa distribution) and 3c (two Maxwellian), while one component kappa distribution is used for Figures 3b and 3d. The best fit parameters are also shown (N is the density, T is the temperature, and kappa is the kappa parameter with subscripts c and h denoting the cold and hot components). MIA observations of rapid variations of ion fluxes (d) at 3130 eV/q during 23:29:50–23:30:20 UTC, (e) at 1795 eV/q during 23:31:50–23:32:20 UTC, and (f) at 210 eV/q during 23:40:30–23:41:10 UTC on 1 October 2021. The black lines show the quasi-1 s resolution data, while the blue lines show the nominal 4 s resolution data. The horizontal bars in Figures 3f and 3g denote the proton gyroperiod (T_{gp}) and the proton gyroradius divided by the spacecraft velocity (r_{gp}/V_{SC}) according to the magnetic field magnitude predicted from the KT17 model. In all panels, the error bars indicate uncertainties due to counting statistics.

Figure 1.

2021-10-01/23:05 ->
2021-10-01/23:45



B-line surface mapping
(dashed: open-closed boundary)

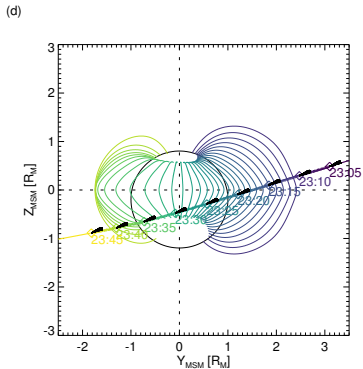
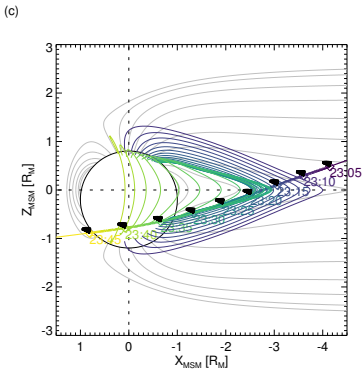
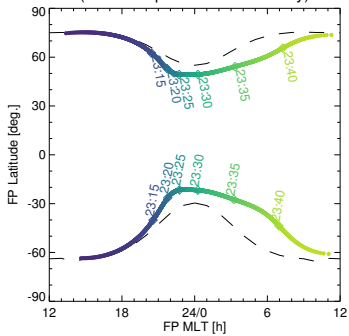


Figure 2.

BepiColombo Mio Mercury Flyby 1

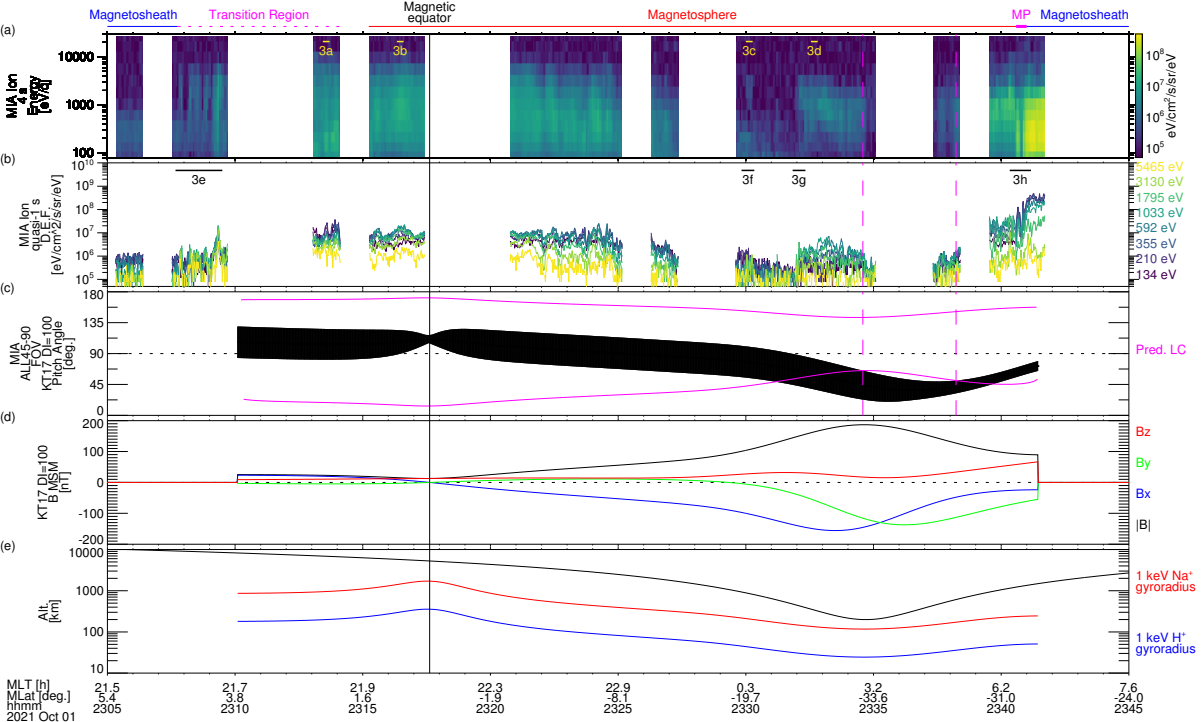


Figure 3.

